Radiological Physics and Technology (2023) 16:102–108
https://doi.org/10.1007/s12194-023-00702-9

RESEARCH ARTICLE

Monte Carlo simulation study to explore optimum conditions for Astatine-211 SPECT

Akihiko Takahashi[1] · Ryosuke Kajiya[2] · Shingo Baba[3] · Masayuki Sasaki[1]

Received: 13 October 2022 / Revised: 20 January 2023 / Accepted: 21 January 2023 / Published online: 31 January 2023

Abstract
^{211}At is a promising nuclide for targeted radioisotope therapy. Direct imaging of this nuclide is important for in vivo evaluation of its distribution. We investigated suitable conditions for single-photon emission computed tomography (SPECT) imaging of ^{211}At and assessed their feasibility using a homemade Monte Carlo simulation code, MCEP-SPECT. Radioactivity concentrations of 5, 10, or 20 kBq/mL were distributed in six spheres in a National Electrical Manufactures Association (NEMA) body phantom with a background of 1 kBq/mL. The energy window, projection number, and acquisition time were 71–88 keV, 60, and 60 s, respectively, per projection. A medium-energy collimator and three low-energy collimators were tested. SPECT images were reconstructed using the ordered subset expectation maximization (OSEM) method with attenuation correction (Chang method) and scatter correction (triple-energy-windows method). Image quality was evaluated using the contrast-to-noise ratio (CNR) for detectability and the contrast recovery coefficient (CRC) for quantitavity. The low-energy, high-sensitivity collimator exhibited the best detectability among the four types of collimators, with a maximum CNR value of 43. In contrast, the low-energy, high-resolution collimator exhibited excellent quantitavity, with a maximum CRC value of 102%. Scatter correction improved the image quality. In particular, the CRC value almost doubled after scatter correction. The detection of spheres smaller than 20 mm in diameter was difficult. In summary, low-energy collimators were suitable for the SPECT imaging of ^{211}At. In addition, scatter correction was extremely effective in improving the image quality. The feasibility of ^{211}At SPECT was demonstrated for lesions larger than 20 mm.

Keywords Astatine-211 · SPECT · Targeted alpha-particle therapy · Thyroid cancer

1 Introduction

^{211}At is an alpha-emitter nuclide that has been used in targeted alpha-particle therapy for cancers such as ovarian cancer [1–3]. Figure 1 shows the decay scheme of this nuclide. Alpha particles possess large emission energies (5–9 MeV) and extremely short path lengths (40–100 µm) compared to beta particles; therefore, linear energy transfer is significantly large [4–8]. The advantage of alpha particles lies in their ability to concentrate energy on an extremely small tumor without affecting normal tissue. Astatine belongs to the halogen family, and its chemical properties resemble those of iodine; therefore, it may be a promising nuclide for the radiotherapy of thyroid cancer instead of the beta-emitter ^{131}I [3].

Owing to the increasing expectations for the clinical application of ^{211}At, its direct imaging for *the* in vivo evaluation of alpha-particle dosimetry has gained importance. Because the path length of alpha particles is extremely short, the distribution of the administered radioactive drug corresponds to the distribution of the absorption of alpha particles. After alpha decay, ^{211}At emits X-rays between 70 and 90 keV and a few gamma rays that are available for the evaluation of alpha-particle dosimetry. ^{211}At imaging has recently been attempted using Compton cameras [9, 10]. However, the intensity of high-energy gamma rays (570 keV), which was targeted in the Compton camera

✉ Akihiko Takahashi
takahashi.akihiko.186@m.kyushu-u.ac.jp

1 Division of Medical Quantum Science, Department of Health Sciences, Kyushu University, Maidashi 3-1-1, Higashi-Ku, Fukuoka, Japan

2 Kyushu Central Hospital of the Mutual Aid Association of Public School Teachers, Shiobaru 3-23-1, Minami-Ku, Fukuoka, Japan

3 Department of Clinical Radiology, Kyushu University Hospital, Maidashi 3-1-1, Higashi-Ku, Fukuoka, Japan

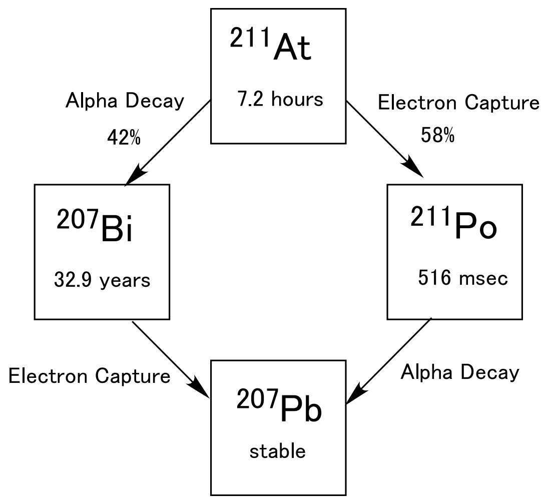

Fig. 1 Decay scheme of ^{211}At

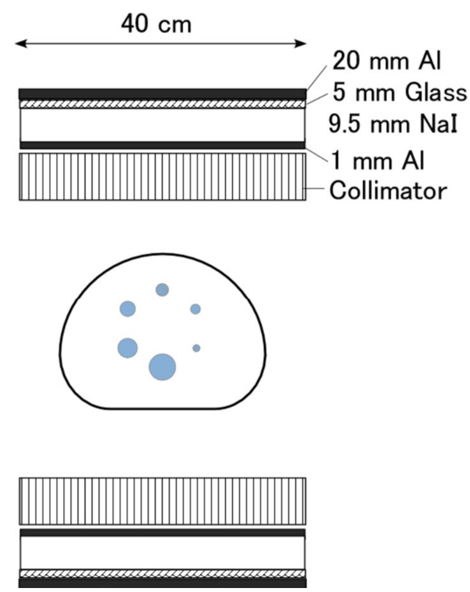

Fig. 2 Setup of a gamma camera for the simulation and cross-sectional view of the phantom

study, has been shown to be considerably low for imaging [10]. Therefore, currently, conventional gamma camera equipment will be promising.

Several researchers have already reported single-photon emission tomography (SPECT) of ^{211}At [11–14]. In these studies, X-rays of approximately 80 keV were detected using a medium-energy collimator. The deterioration of the image quality owing to scattering photons and characteristic X-rays from the lead collimator is a drawback. In the case of radium-223 (^{223}Ra), when X-rays of 84 keV are used for imaging with a low-energy collimator, many characteristic X-rays pass through the energy window and disturb the image. This problem can be partially resolved using a medium-energy collimator with a thicker septum [15–17]. Thus, the choice of collimator is an important factor in obtaining a suitable image [18, 19]. In addition, attenuation and scatter corrections affect the image quality and feasibility of SPECT imaging. Few studies have been conducted on SPECT imaging of ^{211}At [11–14]. Turkington et al. conducted the first study on SPECT imaging of ^{211}At and concluded that a medium-energy collimator is optimal [11]. Subsequent studies used medium-energy collimators with reference to their conclusion [12–14]. However, investigations for the optimum collimator appear insufficient because they focus only on the energy spectrum. Furthermore, the effect of correction on the image quality has not yet been quantified.

In this study, we investigated the optimal conditions for producing ^{211}At SPECT images and the feasibility of using Monte Carlo simulations. Simulation studies are advantageous because they allow the testing of various conditions and settings and provide information that is unavailable in experiments. In this study, we focused on the impact of the collimator, attenuation correction (AC), and scatter correction (SC) on the image quality.

2 Materials and methods

The Monte Carlo simulation used in this study was the MCEP-SPECT model [20], which is based on the gamma camera simulation codes HEXAGON and NAI developed by Tanaka et al. [21]. The simulation setup is shown in Fig. 2. A National Electrical Manufacturers Association (NEMA) body phantom containing six spheres of different diameters (37, 28, 22, 17, 13, and 10 mm) was used. Two gamma cameras were placed 26 cm from the center of the phantom. The phantom was filled with water with a radioactivity concentration of 1 kBq/mL, and six spheres were filled with radioactivity concentrations of 5, 10, and 20 kBq/mL. The projection number was 60 (separation angle: 6°), and the acquisition time was 60 s per direction (total acquisition time: 30 min).

Table 1 presents the radiation used in the simulation model. The main radiation is of 79.29 keV, and thus, the energy window was set to 71–88 keV (± 10%). Two radiations at 569.6 keV and 897.8 keV are attributed to polonium-211 (^{211}Po), the daughter nuclide of ^{211}At. Table 2 lists the dimensions of the collimators used in the simulation. Three collimators were used for low-energy and one for medium-energy.

The projection data were preprocessed using the Butterworth filter (order: 8 and cutoff frequency: 0.5 cycle/cm) and reconstructed using the ordered subset-expectation

Table 1 List of radiations

Energy (keV)	Intensity/decay
76.86	0.127
79.29	0.211
89.8	0.0952
149.7	5.02×10^{-7}
222.7	3.55×10^{-7}
669.8	3.68×10^{-5}
687.0	2.61×10^{-3}
742.7	1.04×10^{-5}
892.4	1.42×10^{-6}
569.6*	3.11×10^{-3}
897.8*	3.21×10^{-3}

*Radiation from Polonium-211 (^{211}Po)

Table 2 Dimensions of collimators

	Septal thickness [cm]	Hole diameter [cm]	Hole length [cm]	Aspect ratio
LEHR[a]	0.03	0.18	4.0	22
LEHS[b]	0.05	0.34	3.6	11
LEGP[c]	0.017	0.178	4.0	23
MEGP[d]	0.108	0.337	4.0	12

Aspect ratio = hole length/hole diameter

[a]*LEHR* low-energy high-resolution

[b]*LEHS* low-energy high sensitivity

[c]*LEGP* low-energy general-purpose

[d]*MEGP* medium-energy general-purpose

maximization (OSEM) method with subsets 6 and 10. Attenuation and scattering corrections were applied to improve the image quality. The Chang method with an attenuation coefficient of 0.182 cm^{-1} was used for attenuation correction [11]. The triple-energy-window (TEW) method, in which the upper and lower energy windows are 88–96 keV and 63–71 keV, respectively, was used for scatter correction. These processes were performed using Prominence Processor Version 3.1, a software package for research and education in nuclear medicine [22].

The SPECT images were evaluated based on two quantitative indices: contrast-to-noise ratio (CNR) and contrast recovery coefficient (CRC). The CNR is expressed as.

$$\mathrm{CNR} = \frac{C_{\mathrm{H}} - C_{\mathrm{B}}}{SD_{\mathrm{B}}}, \tag{1}$$

where C_{H} and C_{B} denote the mean counts inside the region of interest (ROI) of the hot area and ten ROIs of the background areas, respectively, and SD_{B} denotes the standard deviation of the counts inside the background ROIs. CNR, which is the ratio of the net magnitude of the signal in the hot area to the fluctuation of the background, indicates the detectability of the hot area. This area was detectable when the CNR value exceeded 5.

The CRC is expressed as.

$$\mathrm{CRC} = \frac{C_{\mathrm{H}}/C_{\mathrm{B}} - 1}{R_{\mathrm{HB}} - 1} \times 100(\%), \tag{2}$$

$$R_{\mathrm{HB}} = \frac{A_H}{A_B},$$

where A_{H} and A_{B} denote the activity concentrations of the hot sphere, and background, respectively, and R_{HB} denotes the ratio of the hot concentration to the background. CRC indicates the measurement and quantitative accuracies of the activity. The distribution of the ten background ROIs is shown in Fig. 3.

3 Results

Figure 4 shows SPECT images ($R_{\mathrm{HB}} = 20$) with both attenuation and scatter corrections. The image with the low-energy high-resolution (LEHR) collimator is the clearest, and the outline of the hot sphere is clearly visible.

Figure 5 shows the CNR values for each sphere and each ratio of hot to background concentrations. The low-energy high-sensitivity (LEHS) collimator exhibited the highest detectability among the four types of collimators, with a maximum CNR value of 43. However, the CNR value decreased rapidly with decreasing sphere size. The LEHR collimator generally demonstrated better detectability and was detectable (CNR > 5) in a 13-mm sphere.

Figure 6 shows the CRC values. The LEHR collimator exhibited excellent quantitativity, and the maximum CRC value was approximately 100%. The performance of the LEHS collimator was inferior in terms of quantitativity.

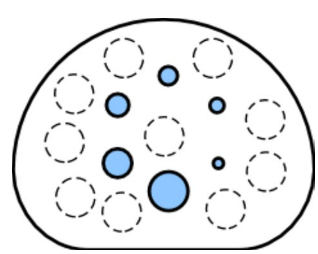

Fig. 3 Regions of interest used in the calculation of the CNR and CRC. The solid and dashed circles represent the hot and background areas, respectively

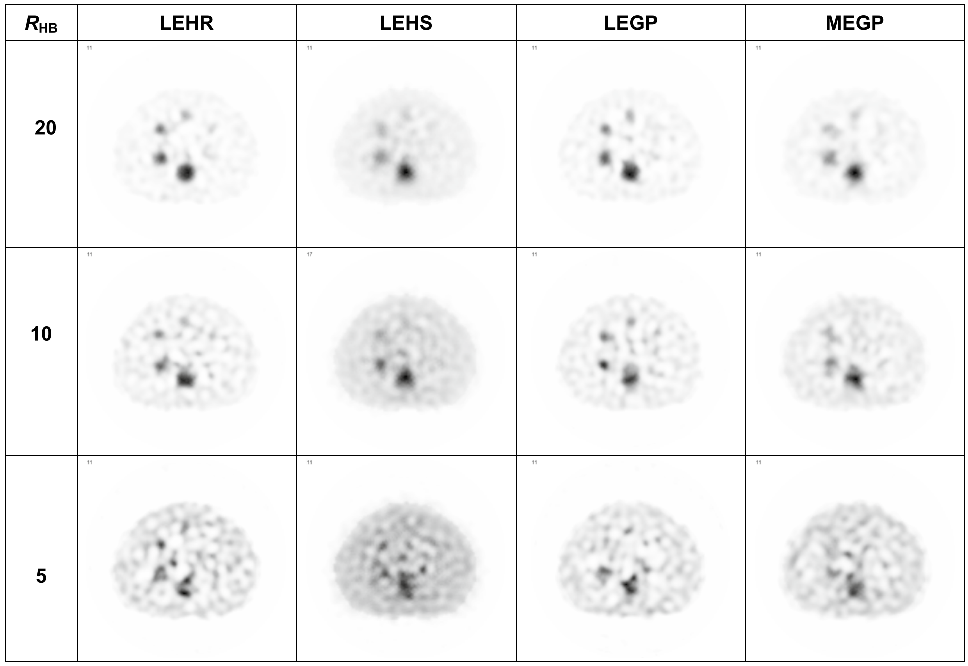

Fig. 4 Simulated SPECT images for $R_{HB} = 20, 10, 5$

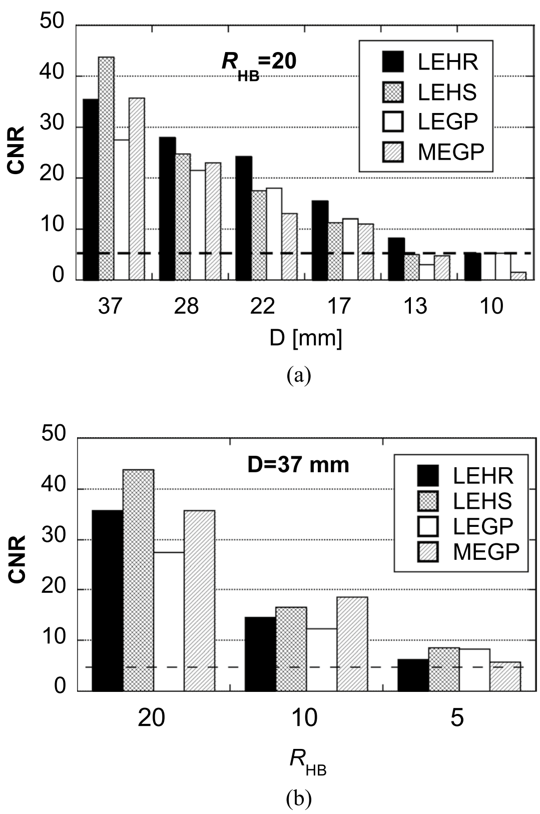

Fig. 5 CNR values for **a** each sphere size and **b** each ratio of hot to background concentration. The dashed line represents the threshold of detection (CNR = 5)

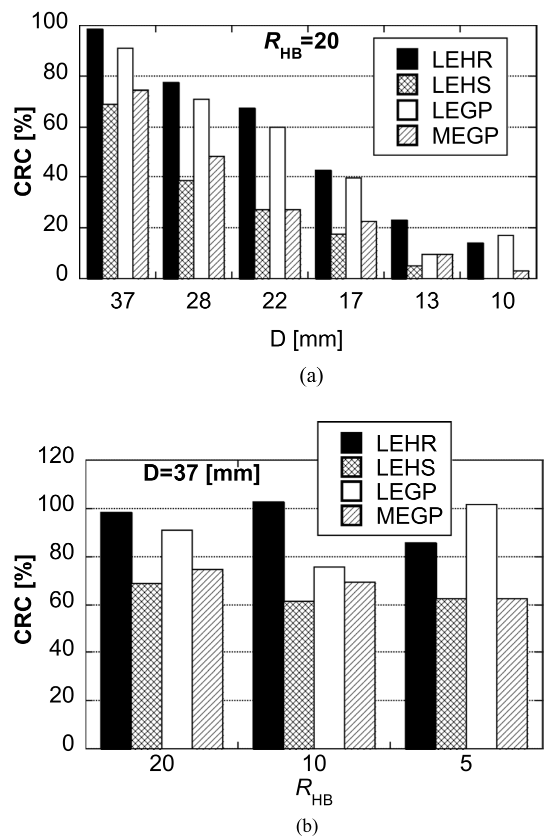

Fig. 6 CRC values for **a** each sphere size and **b** each ratio of hot to background concentration

The low-energy general-purpose (LEGP) collimator performed better than LEHS.

The aforementioned results were obtained using both attenuation and scatter corrections. To assess the impact of scatter correction, Fig. 7 shows the results with only attenuation correction and those with both attenuation and scatter correction. Both the CNR and CRC values improved for all collimators when both corrections were used. In particular, the CRC values doubled when the scatter correction was used. The scatter correction was more effective in improving the CRC value (quantitativity) than the CNR value (detectability).

To consider these characteristics, Fig. 8 shows the partial sensitivity of projection data. The partial sensitivity indicates the counts per source radioactivity (counts/MBq) in each photon detection process denoted as "dir0," "dir1," "indir," and "Pb-X." In Fig. 8, "dir0" denotes the detection process of photons passing through the collimator hole without interacting with the phantom. The detection of photons that interact with the phantom but pass through the collimator hole without interacting with the collimator wall is indicated as "dir1." The process that collide with, penetrate, or interact with the collimator wall irrespective of whether they interact with the phantom are shown as "indir," and "Pb-X" denotes characteristic X-rays from lead [21]. Such "partial sensitivity" cannot be measured experimentally.

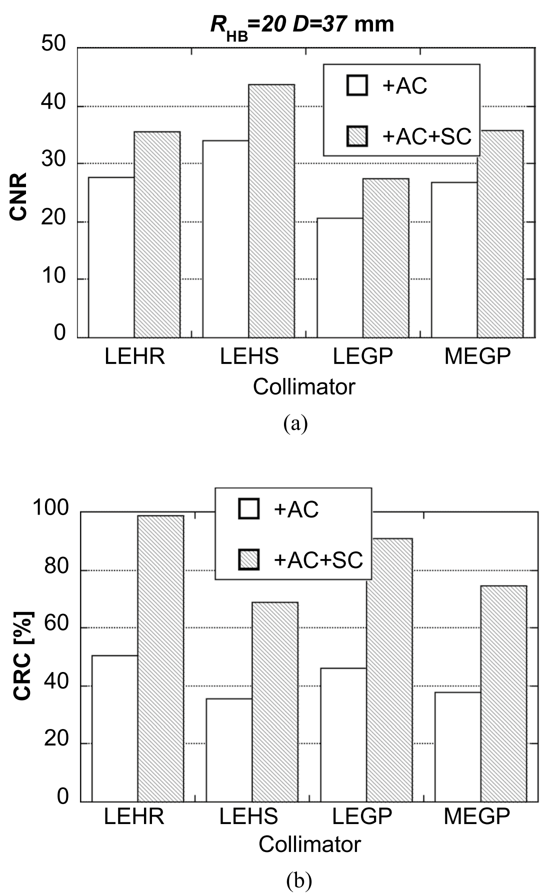

Fig. 7 Impact of attenuation correction (AC) and scatter correction (SC) on **a** CNR and **b** CRC values

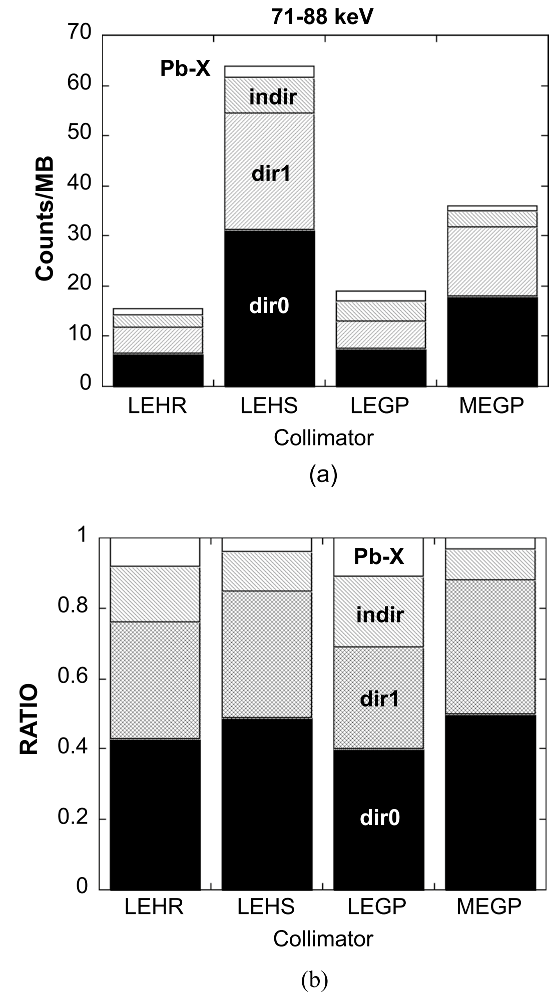

Fig. 8 **a** Partial sensitivities (cps/MBq) in the window of 77–88 keV and **b** ratio of the partial sensitivity to the total sensitivity

The ratios of the "dir0," "dir1," "indir," and "Pb-X" components to the total sensitivity were 40–50%, 30–40%, 10–20%, and 3–10%, respectively. The total sensitivity was the highest for the LEHS collimator. The ratios of "indir" and "Pb-X" of the LEHR and LEGP collimators were larger than those of the other collimators.

4 Discussion

The results in Figs. 5 and 6 show that the collimators in this study performed well when the hot-to-background ratio (R_{HG}) was high and the sphere size was large. However, even the detection of the 37-mm-sphere became difficult when the R_{HG} decreased to 5. The performance of the LEHS and medium-energy general-purpose (MEGP) collimators deteriorated more rapidly as the size of the spheres decreased.

The collimator performance depends on the dimensions, particularly the aspect ratio, which is the ratio of the length to the hole diameter [23]. A collimator with a large aspect ratio effectively blocks photons that do not enter perpendicular to the detection surface. This results in less sensitivity, less blurring of the image, and higher resolution. The aspect ratio of the LEHR and LEGP collimators was 20 or more, whereas those of the LEHS and MEGP collimators were approximately 10. Therefore, the CRC values for the LEHR and LEGP collimators were higher than those for the LEHS and MEGP collimators. The images generated by a collimator with a large aspect ratio have less spread owing to blurring and less leakage of counts from the ROI, resulting in a larger CRC value. A low aspect ratio yields a low spatial resolution. The CNR values for the LEHS and MEGP collimators were high for large spheres; however, the CNR value decreased rapidly with decreasing sphere size owing to the low resolution.

Our study revealed that the effect of scatter correction was particularly significant. The scattered photons blur the image and increase the background count (C_B in Eq. 2), resulting in a reduced CRC value. Because X-rays of 80 keV are used for ^{211}At SPECT, the scattered photons have a significant impact. As shown in Fig. 8, the components of the scattered ("dir1") and direct photons ("dir0") were approximately equal. The count leaks from the ROI were effectively removed, and the CRC value was significantly improved by removing these large numbers of scattered photons. On the other hand, scatter correction reduced C_B and increased SD_B, resulting in increased background noise. However, the contrast of the hot area (C_H–C_B) improved, and the CNR value consequently increased for the setting in this study. To improve quantification, scatter correction is important and necessary.

Another problem with ^{211}At SPECT is the effect of characteristic X-rays emitted from the lead collimators and scattered photons in the collimators. The energy of the characteristic X-rays was approximately 77 keV; this was within the main energy window. The "Pb-X" component cannot be removed by scatter correction; therefore, the image quality is not improved. In ^{223}Ra imaging using a low-energy collimator, a large number of characteristic X-rays disturb the image. This difficulty can be partially resolved using a medium-energy collimator with a thicker septum. MEGP and high-energy general-purpose (HEGP) collimators have been reported to be suitable for imaging ^{223}Ra [16, 17]. In contrast, low-energy collimators performed well for ^{211}At imaging because ^{211}At emits fewer high-energy gamma rays that generate characteristic X-rays. The emission intensities of high-energy gamma rays presented in Table 2 are two to six orders of magnitude lower than those of X-rays (in the case of ^{223}Ra, the difference is within one order of magnitude). The component of the characteristic X-ray ("Pb-X") shown in Fig. 8 is approximately 10% or less; this is considerably less than the 30–40% of ^{223}Ra [16]. For the same reason, the effect of the scattered radiation from the collimator is small. The "indir" component for low-energy collimators is 10–20%; this is half that of ^{223}Ra [16] and one third that of ^{123}I [21]. Finally, the "Pb-X" and "indir" components within the main energy window depend on the intensity of high-energy γ-rays. ^{211}At produces less high-energy gamma rays than ^{223}Ra and ^{123}I, and the use of low-energy collimators is possible for ^{211}At.

The first SPECT imaging study on ^{211}At concluded that the optimal collimator is a medium-energy collimator because it has a small high-energy tail above the photopeak of 90 keV [11]. This matches with the smallest "indir" for the MEGP collimator, as shown in Fig. 8. However, our study suggested that low-energy collimators were more suitable than medium-energy collimators. As shown in Fig. 6, low-energy collimators (LEHR and LEGP) were superior to MEGP in terms of quantification.

5 Conclusion

Low-energy collimators with high aspect ratios were noted to be suitable for SPECT imaging of ^{211}At. Scatter correction was extremely effective in improving the image quality. The feasibility of ^{211}At was demonstrated for lesions larger than 20 mm.

Declarations

Conflict of interest The authors declare no conflicts of interest related to this study.

References

1. Zalutsky MR, Reardon DA, Akabani G, Coleman R, Friedman AH, Friedman HS, et al. Clinical experience with a-particle–emitting ^{211}At: Treatment of recurrent brain tumor patients with ^{211}At-labeled chimeric antitenascin monoclonal antibody 81C6. J Nucl Med. 2008;49:30–8.
2. Palm S, Bäck T, Aneheima E, Hallqvist A, Hultborn R, Jacobsson L, et al. Evaluation of therapeutic efficacy of ^{211}At-labeled farletuzumab in an intraperitoneal mouse model of disseminated ovarian cancer. Trans Oncol. 2021;14: 100873.
3. Watabe T, Nashima KK, Liu Y, Shirakami Y, Ooe K, Toyoshima A, et al. Enhancement of ^{211}At uptake via the sodium iodide symporter by the addition of ascorbic acid in targeted a-therapy of thyroid cancer. J Nucl Med. 2019;60:1301–7.
4. Poty S, Francesconi LC, McDevitt MR, Morris MJ, Lewis JS. α-emitters for radiotherapy: from basic radiochemistry to clinical studies—Part 1. J Nucl Med. 2018;59:878–84.

5. Poty S, Francesconi LC, McDevitt MR, Morris MJ, Lewis JS. α-emitters for radiotherapy: from basic radiochemistry to clinical studies—Part 2. J Nucl Med. 2018;59:1020–6.
6. Kozempel J, Mokhodoeva O, Vlk M. Progress in targeted alpha-particle therapy. What we learned about recoils release from in vivo generators. Molecules. 2018;23:581–98.
7. Trujillo-Nolasco M, Morales-Avila E, Cruz-Nova P, Katti KV, Ocampo-García B. Nanoradiopharmaceuticals based on alpha emitters: recent developments for medical applications. Pharmaceutics. 2021;13:1123–56.
8. Nelson BJB, Andersson JD, Wuest F. Targeted alpha therapy: progress in radionuclide production, radiochemistry and applications. Pharmaceutics. 2021;13:49–76.
9. Nagato Y, Yamaguchi M, Watanabe S, Ishikawa N, Kawachi N, Watanabe H. Astatine-211 imaging by a Compton camera for targeted radiotherapy. Appl Radiat Isot. 2018;139:238–43.
10. Omata A, Kataoka J, Fujieda K, Sato S, Kuriyama E, Kato H, et al. Performance demonstration of a hybrid Compton camera with an active pinhole for wide-band X-ray and gamma-ray imaging. Sci Rep. 2020;10:14064.
11. Turkington TG, Zalutsky MR, Jaszczak RJ, Garg PK, Vaidyanathan G, Coleman RE. Measureing astatine-211 sidributions with SPECT. Phys Med Biol. 1993;38:1121–30.
12. Johnson EL, Turkington TG, Jaszczak RJ, Gilland DR, Vaidyanathan G, Greer KL, et al. Qunantitation of ^{211}At in small volumes for evaluation of targeted radiotherapy in animal models. Nucl Med Biol. 1995;22:45–54.
13. Cederkrantz E, Andersson H, Bernhardt P, Ba¨ck T, Hultborn R, Jacobsson L, et al. Absorbed doses and risk estimates of ^{211}At-MX35 F(ab')2 in intraperitoneal therapy of ovarian cancer patients. Int J Radiation Oncol Biol Phys. 2015;93:569–76.
14 Andersson H, Cederkrantz E, Ba¨ck T, Divgi C, Elgqvist J, Himmelman J, et al. Intraperitoneal α-particle radioimmunotherapy of ovarian cancer patients. Pharmacokinetics and dosimetry of 211At-MX35 F(ab')2—A phase I study. J Nucl Med. 2009;50:1153–60.
15. Takahashi A, Miwa K, Sasaki M, Baba S. A Monte Carlo study on ^{223}Ra imaging for unsealed radionuclide therapy. Med Phys. 2016;43:2965–74.
16 Takahashi A, Baba SM. Assessment of collimators in radium-223 imaging with channelized Hotelling observer: a simulation study. Ann Nucl Med. 2018;32:649–57.
17. Owaki Y, Nakahara T, Kosaka T, Fukada J, Kumabe A, Ichimura A, et al. Ra-223 SPECT for semi-quantitative analysis in comparison with Tc-99m HMDP SPECT: phantom study and initial clinical experience. EJNMMI Res. 2017;7:81–91.
18. https://inis.iaea.org/search/search.aspx?orig_q=RN:25073254. Accessed 1994.
19. Liard E, Williams ED. The optimum technique for ^{201}Tl tomography of myocardium: an investigation using phantoms. Phys Med Biol. 1987;32:985–1000.
20. Takahashi A, Himuro H, Yamashita Y, Komiya I, Baba S, Sasaki M. Monte Carlo simulation of PET and SPECT imaging of ^{90}Y. Med Phys. 2015;42:1926–35.
21. Tanaka T, Uehara S, Kojima A, Matsumoto M. Monte Carlo simulation of energy spectra for ^{123}I imaging. Phys Med Biol. 2007;52:4409–25.
22. http://nm.jsrt.or.jp/prominence_dl/book
23. Takahashi A, Funada K, Himuro K, Baba S, Sasaki M. Impact of collimator on DaT-SPECT imaging: Monte Carlo simulation study. Radiol Med Diag Imaging. 2020;2:1–6.